ACTA IMEKO
ISSN: 2221-870X
December 2024, Volume 13, Number 4, 1 - 10

Experimental and Finite Element Analysis approach for torque assessment in CSFH-based microgrippers with different geometries

Gabriele Bocchetta[1], Giorgia Fiori[1], Salvatore A. Sciuto[1], Andrea Scorza[1]

[1] *Department of Industrial, Electronic and Mechanical Engineering, Roma Tre University, Via della Vasca Navale 79, 00146 Rome, Italy*

ABSTRACT
Microgrippers are MEMS devices capable of precise manipulation of objects on a micrometer scale. Few studies in the literature have focused on the dynamic characteristics of microgrippers with capacitive actuators. This work aims to the development of a novel approach that combines experimental measurements with finite element analysis to evaluate the torque exerted by microgrippers characterized by three different geometries. The investigated devices are composed of electrostatic rotary comb-drives and conjugated surface flexure hinges. The microactuators' rotation has been measured by means of an image analysis technique developed by the Authors, employing videos captured by optical microscope equipped with a high-resolution camera, while the hinge stiffness is estimated through numerical simulations. The experimental results of the different geometries confirm the effectiveness of the proposed approach in assessing the torque output of microgrippers' actuators. The results showed a quadratic trend for the torque as a function of the supply voltage, and that doubling the number of comb-drives results in double the torque. Furthermore, the results also validated the numerical model, allowing the implementation of a phy-digital twin of the device that can be used to simulate the behavior of a microgripper under different conditions and empowering their optimization and design refinement.

Section: RESEARCH PAPER

Keywords: Microgripper; MEMS; electrostatic actuators; CSFH; torque assessment

Citation: G. Bocchetta, G. Fiori, S. A. Sciuto, A. Scorza, Experimental and Finite Element Analysis approach for torque assessment in CSFH-based microgrippers with different geometries, Acta IMEKO, vol. 13 (2024) no. 4, pp. 1-10. DOI: 10.21014/actaimeko.v13i4.1747

Section Editor: Roberto Montanini, Università degli Studi di Messina, Italy

Received January 15, 2024; **In final form** May 13, 2024; **Published** December 2024

Corresponding author: Gabriele Bocchetta, e-mail: gabriele.bocchetta@uniroma3.it

1. INTRODUCTION

In the last decades, researchers have increasingly focused their attention and investigation on microelectromechanical systems (MEMS), the spread of which has grown significantly [1], [2]. They offer a wide range of potential applications, especially in the biomedical field [3]-[6]. This is also justified by a growing trend toward the development of MEMS in microassembly and micromanipulation domains [7]-[9]. Among all MEMS devices, microgrippers (MGs) play an important role in the micromanipulation of cells and tissues because of their versatility and ability to grasp, move and release [10]-[12].

MGs can be classified according to the operating principle of the actuator into five main categories, i.e., piezoelectric [13], shape memory alloy [14], electrostatic [15], electromagnetic [16], and electrothermal devices [17]. Electrostatic actuated MGs have been the subject of extensive research due to their potential for precise manipulation of objects on a micrometre scale. In order to close the gripper jaws and grasp items, these MGs use comb-driven microactuators, which have three distinct structures in terms of transverse [18], [19], lateral [20], [21], and rotary comb-drives [22]-[24], which are driven by electrostatic forces. While electrostatic actuation offers numerous advantages, accurately evaluating the torque exerted by these MGs remains a challenge. In this regard, the present study focuses on electrostatic actuation-based MGs equipped with Conjugate Surface Flexure Hinges (CSFHs) and rotary comb-drive microactuators [25]-[29]. A sketch of a portion of the MG structure with CSFHs and rotary comb-drives is shown in Figure 1.

From the results in the literature, it can be stated that rotary comb-drives can move following a trajectory as close to an ideal rotation if the hinges have a circular geometry such as CSFHs [30]. Moreover, MG architectures with a single pair of hinges perform greater displacements than more complex architectures

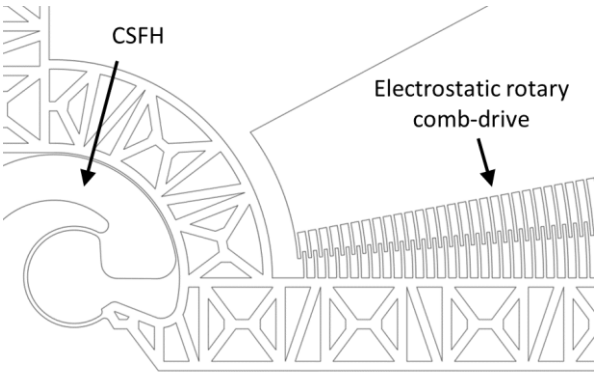

Figure 1. CAD detail of a micrograpper with CSFHs and rotary comb-drives.

(e.g., prototypes based on a double four-bar linkage geometry in a mirror configuration) with the same supply voltage [31], [32].

In this context, the present study aims to assess the torque exerted by rotary microactuators of three MGs with different geometries. This issue is necessary and crucial to ensure accuracy and safety during micromanipulation tasks, since from torque assessment, the measurement of the force between the two MG jaws can be derived [33]. The exerted torque has been evaluated through a hybrid method that combines the experimental analysis with numerical simulations based on Finite Element Analysis (FEA) starting from the displacement of the microactuator as a function of the supply voltage. Displacements have been experimentally evaluated by measurements made through an innovative method developed by the authors and based on image analysis of videos. The latter have been acquired by a trinocular optical microscope equipped with a high-resolution and high fps camera. On the other hand, the stiffness coefficient of the curved beams, constituting the CSFHs, has been estimated through numerical simulations. In addition, based on the characterization of the single-joint MG geometry composed of a single CSFH and comb-drives pair [34], the other multi-joint MG geometries constituted by a double four-bar linkage geometry have also been analysed. The goal of the proposed approach is to validate the simulated MG model and then implement a phy-digital twin useful for both nondestructive analysis and the development of new optimized designs.

The paper is organized as follows. Section 2 describes the main components of the setup for the experimental analysis to measure the displacements of the devices under test and the main steps in processing the acquired videos and numerical simulations. Section 3 describes the method adopted for estimating the uncertainties in torque calculation, while in Section 4 the results of torque assessment, for different MG geometries, are reported with a discussion on the comparison between the values obtained experimentally and by simulation and the effect of the comb-drive number on the applied torque. Finally, in Section 5, a summary of the findings and directions for future research are presented.

2. MATERIALS AND METHODS

The devices investigated in this study are three MG prototypes with different geometries (named G1, G2 and G3) actuated by rotary comb-drives and equipped with CSFHs. The first is a single-joint model consisting of a single pair of comb-drives and hinges, hereinafter referred to as G1 (Figure 2a) [35], [36]. The other two are multi-joint models characterized by a double four-bar linkage architecture in mirror configuration consisting of 8 CSFHs [31], [37]. The difference between these prototypes lies in the number of comb-drives, i.e., a single comb-drive pair for the geometry named G2 (Figure 2b) and two comb-drive pairs for the geometry named G3 (Figure 2c). The three MGs have been monolithically manufactured with a DRIE (Deep Reactive Ion Etching) process [38]-[40] on the same Silicon-On-Insulator (SOI) wafer [41] with a rigid aluminium mask. The wafer used for the fabrication of the MGs has a device thickness of 40 μm, and both capacitive microactuators and CSFHs feature the same design specifications, listed in Table 1.

The proposed method for torque assessment is based on the combined approach of experimental tests and finite element analysis and is divided into three main phases. The first stage is based on the experimental approach, through which a kinematic characterization of the three devices under test has been carried out by analysing the displacement of the main components as a function of supply voltage. After that, on the basis of the experimentally obtained results, the FEA approach has been conducted, by which the stiffness coefficient of the curved beams of CSFHs has been estimated. Lastly, the torque applied by the microactuators has been assessed by considering the

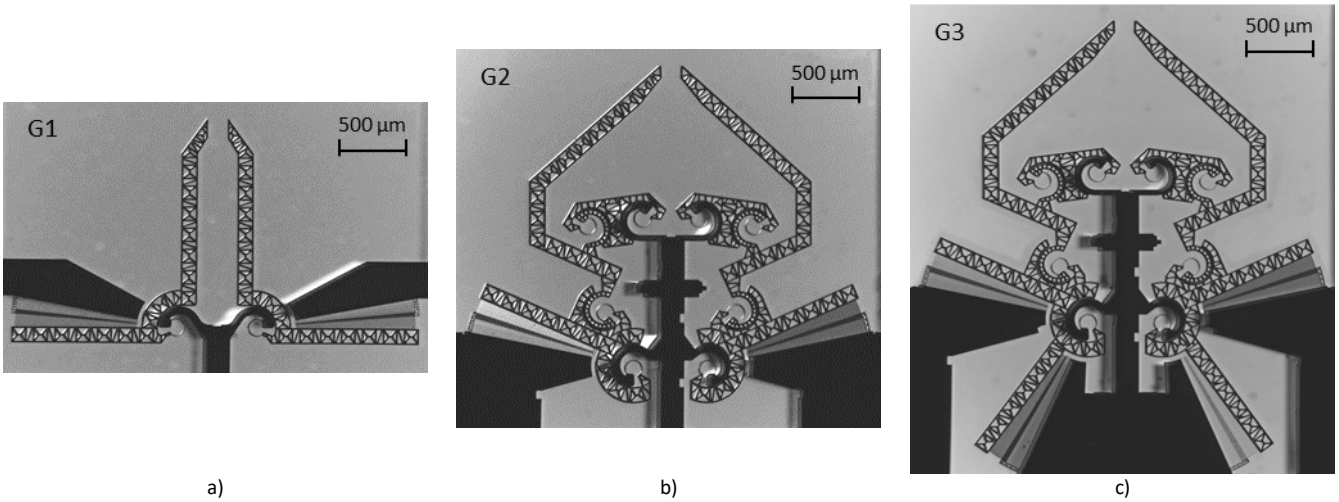

a) b) c)

Figure 2. Micrograppers with three different geometries: a) single-joint geometry (G1), double four-bar linkage geometries with b) two comb-drives (G2) and c) four comb-drives (G3).

Table 1. Microgrippers main design specifications.

Component		G1	G2	G3
Comb-drive	Number of comb-drives	2	2	4
	Number of fingers per comb-drive		64	
	Finger distance		10 µm	
	Rotor-Stator finger distance		3 µm	
	Finger width		4 µm	
	Finger minimum length		38 µm	
	Finger maximum length		151 µm	
	Initial overlapping angle		2°	
	Comb-drive thickness		40 µm	
CSFH	Number of CSFH	2	8	8
	Curved beam length		252 µm	
	Curved beam width – h		5 µm	
	Neutral axis curvature radius – r_n		62.5 µm	
	Curved beam subtended angle – α		240.9°	
	Conjugate surfaces clearance		2 µm	
	Curved beam thickness – b		40 µm	

equilibrium with the resisting torque due to the hinges' deformation, evaluated through the variables calculated in the previous steps. In the following subsections, each of these phases is described in detail and the main steps are summarized in the block diagram shown in Figure 3.

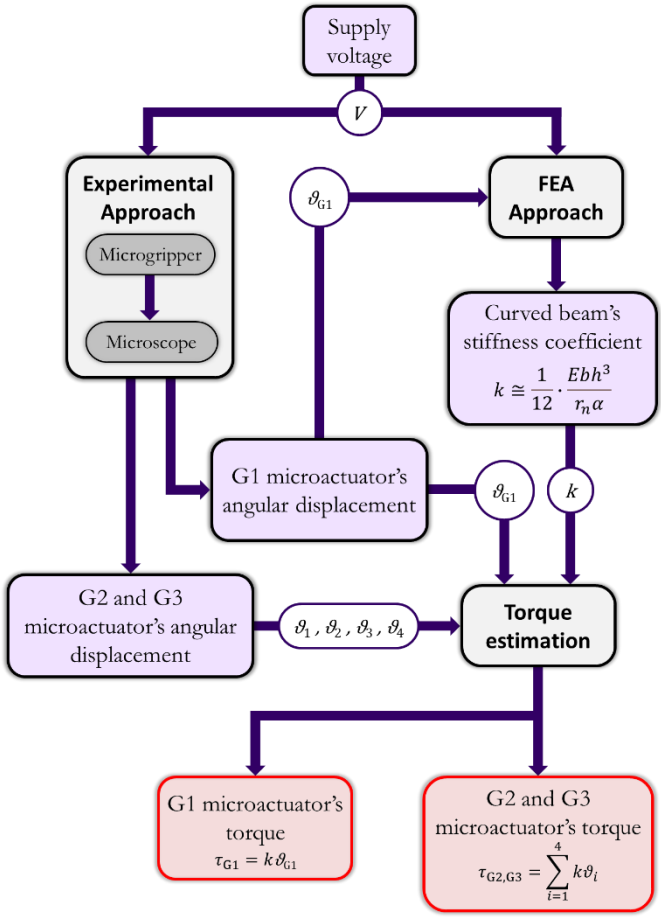

Figure 3. Block diagram including the main steps of the proposed method for assessing the torque exerted by microgrippers.

Table 2. Experimental setup main components.

Device	Characteristics
Function Generator	Amplitude: 0 to ± 10 V peak-to-peak, Frequency: 0.01 µHz to 5 MHz
Power amplifier	Amplitude: 0 to ± 20 V
Micropositioners	Travel range (X/Y/Z): 10 mm Screw resolution (X/Y/Z): 500 µm
Trinocular optical microscope	Zoom: 16×, 20×, 40×, 60×, 80×, 100×
Video camera	23.3 MP, sensor size ½.3 in, maximum video resolution, and fps: 4K (3840×2160 pixels) at 120 fps
Video processing software	In-house algorithm implemented in MATLAB (2022b, MathWorks)
PC	Intel® Core i7-11370H, 32 GB RAM, NVIDIA® RTX™ 3050 Ti

2.1. Experimental approach

The angular displacement of the microactuators has been measured by processing videos acquired through a high-resolution camera mounted on a trinocular optical microscope. Two different levels of magnification have been set to record videos of each MG prototype. A video at 40× has been acquired to capture the entire comb-drive and two videos at 80× to capture and analyse both the displacement of the gripper tip and the free end of the comb-drive. The experimental setup used in this phase of the study can be divided into two main parts:

1) the instrumentation required to generate the power signal, which includes a function generator, a power amplifier, and micropositioners that allow contact with the MG under test;
2) the image acquisition system constituted by a trinocular optical microscope equipped with a high-resolution camera and framerate [42].

The components of the experimental setup are shown in Figure 4 and listed in Table 2 with their main characteristics. The power instrumentation has been set to generate a trapezoidal ramp signal with a peak-to-peak amplitude in the range of 0-20 V and a period of 2 s. This waveform has been chosen so as to ensure that the devices had stationary phases in both the neutral position and the position corresponding to the maximum supply voltage. Videos, recorded at 60 fps, have a duration to capture at least thirty periods of the power signal. Afterwards, data has been processed and analysed through a custom-written measurement procedure developed in MATLAB environment that allows the measurement of displacements of regions of interest by video tracking of virtual markers identified by corners detection using minimum eigenvalue algorithm [43]. The measurement procedure searches for the corresponding marker by making a

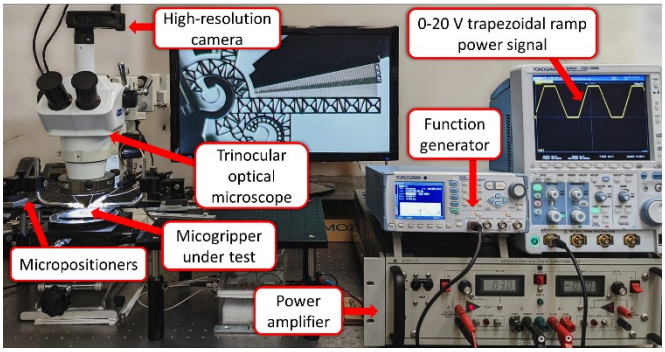

Figure 4. Experimental setup.

comparison between the current frame and each point in the previous frame. Once it has analysed the position of all markers over time, it evaluates the translation, rotation, and scale of the region of interest throughout the duration of the video. The results obtained for the angular displacement of G1 microactuators as a function of different values of supply voltage have been used to numerically estimate the stiffness coefficient k of the CSFH curved beam by implementing a finite element model. Conversely, the results obtained for the comb-drives rotation in G2 and G3 have been used to validate the finite element simulations performed taking into account the corresponding geometry.

2.2. FEA approach

Numerical simulations have been carried out with COMSOL Multiphysics software to simulate MG behaviour under the most realistic conditions. To this aim, both the Solid Mechanics and the Electrostatics modules have been included. The first was to simulate the deformation of the structure and especially the CSFHs. For this purpose, in the Solid Mechanics module, a Quadratic Lagrange discretization and an isotropic material symmetry have been considered. On the other hand, the second module was to reproduce the actual MG working principle and to model the electrostatic forces involved. In this case, a Quintic discretization of the electric potential has been set. To bring together the two previous modules, the electromechanical forces for the coupled interfaces have been added to the study. FEA simulations have been performed using the 2D models of the MGs to which 40 μm out-of-plane thickness has been added. The two-dimensional models are the same as those used during the fabrication process to create the aluminium mask, which has been used to protect the part of the silicon that does not have to be machined with the DRIE process. To accurately simulate the electrostatic actuation of the comb-drives, the model includes the air that surrounds the device as a free-deformation domain, and the geometry of the mesh has been configured for the device's thinner parts as well as the air domain. To obtain an objective comparison among the three mathematical models, the mesh generation has been set with the same specifications, in order to get the same mesh for the microactuators and CSFHs. In particular, triangular elements have been considered with an average quality of 0.8 and the number of elements varying from a minimum of around 65k for G1 to a maximum of around 160k for G3. The material used in the numerical simulations is (100) single crystal silicon, the characteristics of which are consistent with what has been found in the literature [44]-[46], and it corresponds to the material used in the manufacturing procedure of the device. In order to simulate the displacement as a function of different voltage values, a stationary study has been set up with an auxiliary sweep considering 30 values in the range 0-20 V, geometric nonlinearities and a MUMPS solver. The stiffness coefficient of the curved beam has been estimated via FEA following the experimental results obtained for G1. It has been assumed the same for all CSFHs of the three devices under the assumption that they are nominally identical since they not only come from the same SOI wafer and thus the same material but also the same manufacturing process.

2.3. Torque assessment

Since the MGs did not perform manipulation tasks or interact with third-party objects during the experimental tests, every position occupied during motion can be considered an equilibrium between the torque exerted by the microactuators and the elastic resisting torque produced by the deformation of the CSFHs' curved beams. In the G1 design, the comb-drive directly operates against the curved beam, therefore the torque τ_{G1} exerted by the microactuator can be evaluated as follows:

$$\tau_{G1} = k\,\vartheta_{G1}\,, \tag{1}$$

where k is the stiffness coefficient of the curved beam evaluated in Nm·rad^{-1} and determined via FEA, whereas ϑ_{G1} is the experimentally measured rotation of the comb-drive.

As a first approximation, the coefficient k of the curved beam can be estimated for the range of rotation obtained from the comb-drives of G1 as [47], [48]:

$$k \cong \frac{1}{12}\cdot\frac{E\,b\,h^3}{r_n\,\alpha}\,, \tag{2}$$

where E is Young's modulus of silicon, b is the device thickness of 40 μm, h indicates the 5 μm width of the curved beam, r_n represents the curvature radius of the curved beam neutral axis, and α is the angle subtended by the curved beam. Equation (2) can be considered valid under the assumption that the curved beams are homogeneous, linear elastic with uniform and rectangular cross sections, as well as assuming a constant bending moment.

On the other hand, as regards the G2 and G3 geometries, in order to assess the torque exerted by the microactuators, it is necessary to analyse the mechanism configurations. Since G2 and G3 are characterized by a double four-bar linkage in a mirror configuration, the angular displacements of the other members of the mechanism have been evaluated by the Newton-Raphson method [49] on the basis of the rotation of the comb-drives, i.e., the crank angle, measured by the experimental tests. In this way, it has been possible to individually estimate the resistant moments due to the deformation of all CSFHs, each of which has been estimated by considering (1). Finally, also for the G2 and G3 geometries, the torque exerted by the comb-drives has been assessed considering the assumption of equilibrium

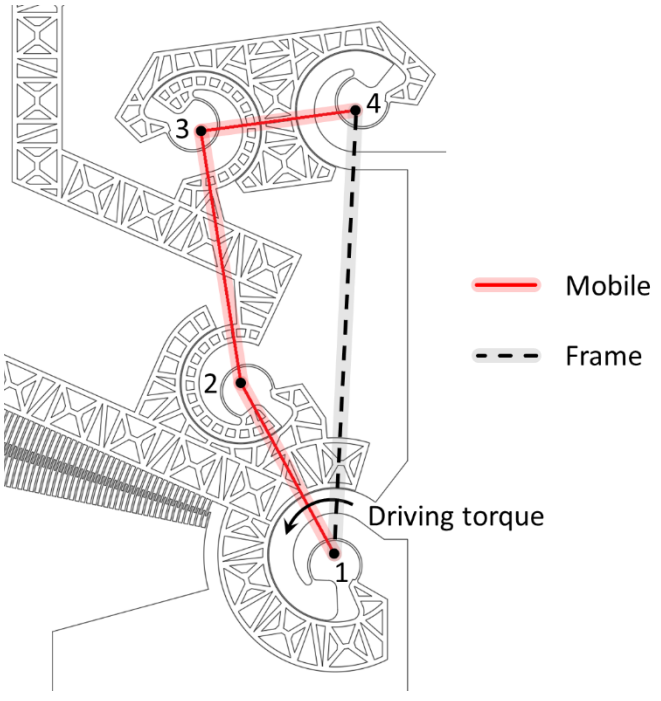

Figure 5. Schematic diagram of the four-bar linkage mechanism on which the G2 and G3 geometries are based and numbering of the hinges.

between the actuation of the comb-drives and the deformation of the CSFHs.

A schematic of the four-bar linkage mechanism on which the G2 and G3 geometries are based is shown in Figure 5. In particular, in the analysis of the equivalent mechanism, CSFHs are replaced by ideal rotary hinges. In addition, from Figure 5, it can also be seen that the centre of rotation of the mechanism members corresponds to the centre of elastic weights of the CSFH [50]-[52]. If the torque applied to the crank is balanced by the resisting torques at the other hinges, the torque exerted by the microactuators can be expressed as:

$$\tau_{G2,G3} = \sum_i k\,\vartheta_i = k\,\vartheta_1 + k\,\vartheta_2 + k\,\vartheta_3 + k\,\vartheta_4\,, \tag{3}$$

where τ is the torque exerted by the microactuator as a function of the comb-drive angular displacement ϑ_1 (as well as the crank angle), and the angles ϑ_2, ϑ_3 and ϑ_4 corresponding to the deformation of the respective CSFHs. It is worth noting that ϑ_i denotes the angle described during rotation and is evaluated as the difference between the value as a function of the supply voltage $\vartheta_i(V)$ and the value in the neutral position $\vartheta_i(0)$:

$$\vartheta_i = \vartheta_i(V) - \vartheta_i(0)\,. \tag{4}$$

3. UNCERTAINTY ANALYSIS

The measurement uncertainty analysis has been carried out by considering different contributions according to the study phase.

First, the main uncertainty sources related to the experimental approach have been determined and their components, i.e., type A and type B uncertainties expressed as standard deviations (SDs), combined in quadrature [53]. Type A uncertainties have been estimated as the dispersion of the experimental outcomes obtained by averaging both gripper tip and comb-drive displacement over a single period of the trapezoidal power signal. On the other hand, type B uncertainty (σ_B) has been estimated by combining the contributions given by the uncertainty sources in the measurement chain (Table 3) as follows:

$$\sigma_B = \sqrt{\left(\frac{\partial d}{\partial V}\sigma_{PS}\right)^2 + \sigma_{OS}^2 + \sigma_M^2}\,, \tag{5}$$

where d indicates the displacement value as a function of the supply voltage V, σ_{PS} is the SD due to the power supply system evaluated as the sum in quadrature of the contributions of the function generator amplitude and the power amplifier amplitude uncertainties, σ_{OS} is the SD related to the optical system including the contributions of both the pixel size and the spatial resolution [54], and σ_M is the SD associated to the measurement procedure of the MG displacements. As in [55], [56], the uncertainty related to a measurement procedure implemented in MATLAB has been estimated through a Monte Carlo Simulation (MCS) with 10^4 iterations for each MG prototype (Table 3). By including different virtual markers at each iteration, the centroid position in the image has been made to vary randomly as a normal distribution with a 2-pixel standard deviation for both x and y coordinates. As regards the estimation of uncertainty related to other four-bar linkage angles, the contribution related to crank angular displacement has been propagated in the analysis of the four-bar linkage configurations by the Newton-Raphson method. In (5), the uncertainty contribution related to the frequency of the generated signal does not appear, as it has been considered negligible since it is several orders of magnitude lower than the others.

Table 3. Main uncertainty sources in the experimental approach.

Source of Uncertainty	Value		
Function generator amplitude [a]	1 % of $V_{peak\text{-}to\text{-}peak}$ + 2 mV		
Function generator frequency [a]	3 ppm of setting + 2 pHz Aging rate: ± 1 ppm/year		
Power amplifier amplitude [a]	2 mV		
Optical system [a]	1 µm		
	G1	**G2**	**G3**
Maximum angular displacement with video tracking measurement procedure [b]	0.01°	0.01°	0.02°
Maximum tip displacement with video tracking measurement procedure [b]	0.3 µm	0.4 µm	0.4 µm

[a] Uncertainty values provided by the instrumentation datasheets; [b] Standard deviation values obtained from Monte Carlo simulations.

On the other hand, the standard uncertainty of the stiffness coefficient outcomes via FEA has been estimated by varying the MG geometric dimensions in (2) through a further MCS (10^4 iterations) [57] in which the uncertainty contribution associated with the DRIE process [27] has been included. The dimensional uncertainty related to the DRIE process of a SOI wafer with 40 µm device thickness can vary depending on several factors, including the specific parameters of the DRIE process, the wafer material properties, and the measurement method used. However, typical values of dimensional uncertainty in DRIE processes for small elements (< 100 µm) are between 1-5 % of the element size. For a 5 µm feature, as in the case of CSFH width, this would correspond to an uncertainty that can range from a few tens of nanometres to a few hundred nanometres [57]-[60].

Finally, the measurement uncertainty of the microactuator torque has been derived by applying the error propagation law, in which the standard uncertainties of the stiffness coefficient and the angular displacements have been included.

4. RESULTS AND DISCUSSION

In this section, results obtained from the experimental phase, i.e., displacements of the three MG geometries, and those from numerical simulations, i.e., hinge stiffness coefficient, are presented and discussed. Moreover, the outcomes of torque applied by the G1, G2 and G3 microactuators are provided. They are expressed as the mean value of the different tests ± SD.

4.1. G1 angular displacement and curved beam stiffness coefficient estimation

The angular displacement of G1 microactuator as a function of the supply voltage is shown in Figure 6. In particular, the rotation trend as the supply voltage increases, for a maximum of 0.80° ± 0.01° at 20 V, is provided (Figure 6a). This rotation corresponds to a maximum displacement of the free end of the comb-drive, which has been experimentally measured to be 17.3 ± 1.1 µm. In Figure 6b the comparison between the neutral comb-drive position (magenta) and the maximum displacement (green) is shown. Similarly, Figure 6c shows the results obtained through numerical simulations for the overall displacement of each MG point, where the maximum displacement (17.1 µm) is displayed in orange in the contour plot. The outcomes obtained for the rotation of G1 microactuators correspond to a maximum

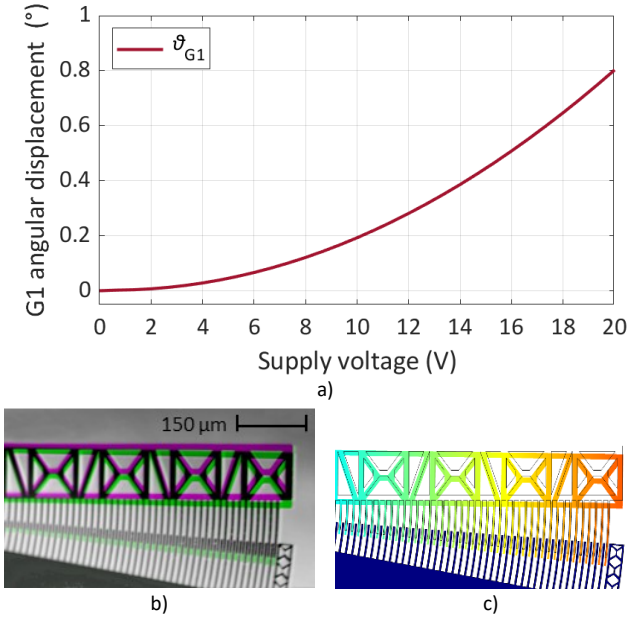

Figure 6. Angular displacement of the comb-drive of G1: a) rotation trend as a function of the supply voltage, and maximum displacement of the free end evaluated by b) experimental approach and c) FEA.

displacement of the gripper jaw tip of 22.1 ± 1.1 µm obtained experimentally, and 21.8 µm by simulation.

Through the numerical analysis performed by simulating the electrostatic actuation of G1 in COMSOL and based on the results for the angular displacement, a stiffness coefficient of the CSFH curved beam has been estimated to be 0.10 ± 0.01 µN·m·rad^{-1}. The latter has been assumed as the stiffness coefficient of all CSFHs for all three geometries under investigation.

4.2. G2 and G3 experimental results and mathematical model validation

Results obtained for the comb-drive rotation of G2 and G3 are shown in Figure 7. In particular, Figure 7a shows the rotation of the comb-drive of G2 (blue) as a function of the supply voltage, as well as the different configurations for the other angles of the four-bar linkage structure. Similarly, Figure 7b shows the results obtained for the rotation of the double comb-drives (green) and the other angles of G3 as a function of the supply voltage. The Newton-Raphson method has been chosen for the evaluation of the configurations for the four-bar linkage architectures as a function of the crank angle, mainly due to the uncertainties due to the optical system that makes it difficult to measure the small displacements (below 1 µm) of the other members of the mechanism.

From the experimental tests, a maximum rotation of 0.16° ± 0.01° has been obtained for G2, and 0.32° ± 0.02° for G3, which correspond to a maximum displacement of the tip of the gripper of 2.6 ± 1.1 µm and 5.1 ± 1.1 µm, respectively, with a supply voltage of 20 V. From these results, it is confirmed that that doubling the number of comb-drives results in a double displacement. This means that, at least in the displacement range considered, the displacement is directly proportional to the number of comb-drives and their geometric characteristics.

The numerical simulations carried out for G1 have been repeated for the other two geometries under the same conditions, such as the same material, mesh, actuation, and stiffness value of the curved beams of the CSFHs. The results

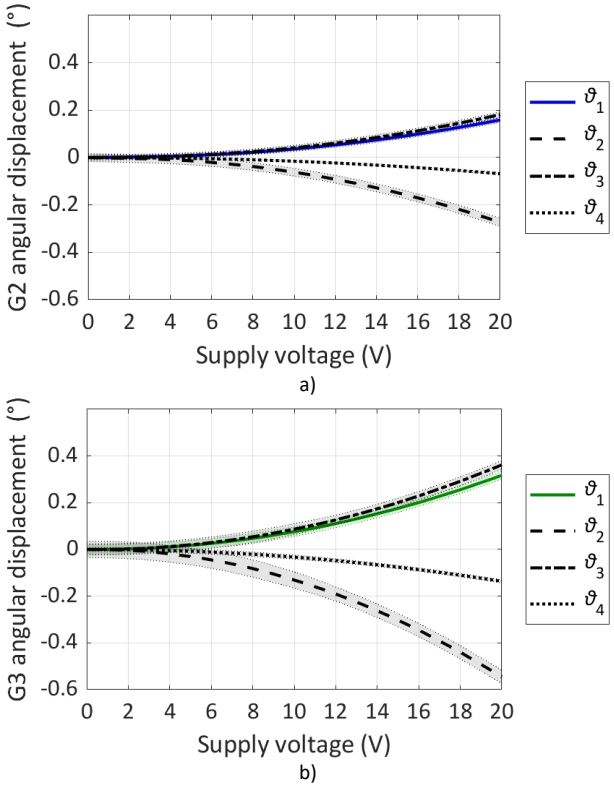

Figure 7. Angular displacement of microgrippers with the four-bar linkage architecture as a function of supply voltage: a) comb-drive rotation of G2 (blue) and trend of the other angles; b) comb-drive rotation of G3 (green) and trend of the other angles.

obtained from the simulations show a maximum rotation of the comb-drive of G2 equal to 0.15° and a maximum displacement of the tip of the grippers of 2.6 µm, while for G3 a rotation of 0.31° for the comb-drives and 5.2 µm for the jaws of the grippers.

The experimental results validate the numerical model implemented in the FEA, and for all displacement values considered for each supply voltage value, an overall mean absolute percentage error of about 10 % has been assessed. It is worth noting that this error is due to small displacements at low voltage values that cause a high error. In this regard, considering voltage values between 10 and 20 V, the overall mean absolute percentage error is about 4 % and does not reach 3 % if only the maximum displacement values are taken into consideration. The computation of the mean absolute percentage error (MAPE) has been carried out by applying the definition as follows:

$$\mathrm{MAPE} = \frac{100}{n}\sum_{i=1}^{n}\left|\frac{x_{\mathrm{EXP}_i} - x_{\mathrm{FEA}_i}}{x_{\mathrm{EXP}_i}}\right|, \tag{6}$$

where x_{EXP} denotes the experimental measurement of displacement and x_{FEA} the corresponding value evaluated through the numerical simulation.

Figure 8 shows the experimental and simulated results for the maximum displacement of the grippers of G2 and G3.

4.3. Results on the assessment of torque applied by the comb-drives of G1, G2 and G3

The torque applied by the comb-drives has been computed using all the rotation values of G1, G2, and G3, as well as the same stiffness value for the curved beams. Table 4 summarizes all of the outcomes from this investigation, while Figure 9

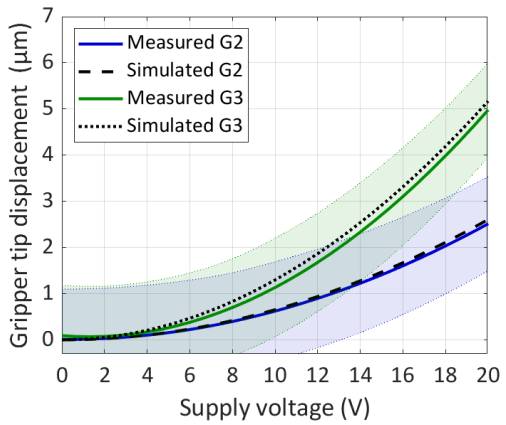

Figure 8. Gripper tip displacement for microgrippers G2 (blue) and G3 (green) in comparison with simulated results.

depicts the evolution of the torque applied by the microactuators as a function of the supply voltage. A maximum torque of 1.4 ± 0.2 nN·m, 1.2 ± 0.2 nN·m, and 2.4 ± 0.3 nN·m has been assessed for G1, G2, and G3, respectively, to deform the structures of the devices by the rotation angle measured for the respective comb-drives. In the scientific literature [61], [62] there are mathematical formulations that describe the electrostatic torque of rotary comb-drives as a function of the square of the applied voltage and the capacitance variation, which in turn depends on the geometric characteristics of the microactuators. This is verified by the results obtained, since the torque applied by the microactuators has a quadratic behaviour as a function of the supply voltage. Moreover, with regard to G1 and G2 geometries, the obtained torque values are compatible since they are actuated by comb-drives with the same geometric characteristics. On the other hand, as also shown from the experimental results obtained for the displacement, the double comb-drives of G3 apply twice the torque compared to devices equipped with single comb-drives.

5. CONCLUSIONS

In this study, a novel method for the assessment of torque exerted by MEMS microgripper actuators for biomedical applications is presented. The results obtained in this study have demonstrated the effectiveness of the combined experimental and finite element approach proposed for the assessment of

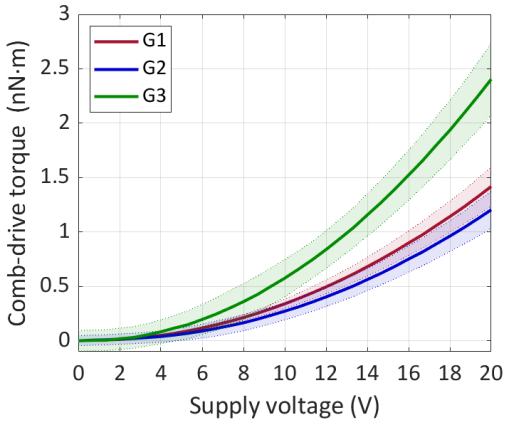

Figure 9. Torque applied by the three microgripper geometries (G1 in red, G2 in blue and G3 in green) as a function of supply voltage.

Table 4. Summary of maximum values. Experimental data are expressed as mean value ± standard deviation.

Parameter	Value		
CSFH Stiffness coefficient (µN·m·rad^{-1})	0.10 ± 0.01		
	G1	**G2**	**G3**
Measured comb-drive maximum angular displacement (°)	0.80 ± 0.01	0.16 ± 0.01	0.32 ± 0.02
Simulated comb-drive maximum angular displacement (°)	0.79	0.15	0.31
Measured gripper tip maximum displacement (µm)	22.1 ± 1.1	2.6 ± 1.1	5.1 ± 1.1
Simulated gripper tip maximum displacement (µm)	21.8	2.6	5.2
Maximum torque applied by comb-drive (nN·m)	1.4 ± 0.2	1.2 ± 0.2	2.4 ± 0.3

torque exerted by MGs with different geometries. In particular, the experimental results, obtained by processing through an *ad hoc* measurement procedure in MATLAB environment the videos of the devices under test, allowed to measure the angular displacement of the microactuators. Data have been acquired through an optical microscope equipped with a high-resolution camera. The results for the rotation of the comb-drive have been used to estimate the stiffness coefficient of the CSFH's curved beam.

The results also validated the finite element model implemented in COMSOL Multiphysics for numerical simulations and have been used to estimate the torque exerted by the microactuators. The validation of the mathematical model obtained through comparison with the experimental results, allowed the implementation of a phy-digital twin of the device that can be used to simulate the behaviour of the system in conditions different from those of the experiments [63]. In this case, the phy-digital twin can be used to simulate applications of MGs, such as the behaviour of the microactuators during the manipulation of objects of different sizes and shapes. In this way, it could be possible to estimate and predict the performance of the microgrippers and identify their optimal operating conditions. The implementation of the phy-digital twin could also be useful for the development and optimization of new designs.

The results obtained showed that the torque exerted by the microactuators has a quadratic trend as a function of the supply voltage and that doubling the number of comb-drives results in a double torque. This result is in agreement with what is reported in the literature [64] both in terms of trend and order of magnitude. In particular, the single-joint MG composed of a pair of comb-drives and a pair of CSFHs can apply a maximum torque of 1.4 ± 0.2 nN·m. This value can be considered compatible with that obtained from the MG characterized by a double-jointed four-bar linkage architecture and also equipped with a single pair of microactuators that is able to apply a maximum torque of 1.2 ± 0.2 nN·m since the comb-drives that actuate it have the same geometric characteristics of the previous model. Regarding the third geometry, the MG is composed of a double-jointed four-bar linkage structure, but differently from the previous device, the actuators are composed of double rotary comb-drives. This geometry can apply a maximum torque of

2.4 ± 0.3 nN·m, which appears double compared to MGs that are actuated by single comb-drives.

In conclusion, the proposed method can be used to estimate the torque exerted by MGs with different geometries, providing an important tool for the design and optimization of these devices. The results obtained in this study represent an important step forward in the development of methods for the assessment of torque exerted by rotary electrostatic microactuators.

In the future, it will be important to extend the method to MGs with more complex geometries and apply it also to devices on a nanometric scale. In addition, the development of a physical-mathematical model capable of describing the deformation of the CSFHs and the torque exerted by the microactuators as a function of the geometric characteristics and materials of the devices could contribute to improving the accuracy of the estimates obtained. Finally, an additional aspect of fundamental interest concerns the implementation of an experimental measurement method of the torque applied by the microactuators. In this way, it would be possible to evaluate the force that the microgrippers are able to apply when they grasp an object or execute micro-scale tasks.

REFERENCES

[1] J. Marek, B. Hoefflinger, U. M. Gomez, MEMS—Micro Electromechanical Sensors for the Internet of Everything, in: CHIPS 2020 VOL. 2. B. Höfflinger (editor). Springer, Cham, 2016, ISBN 9783319220932, pp. 221-229. DOI: 10.1007/978-3-319-22093-2_15

[2] C. Chircov, A. M. Grumezescu, Microelectromechanical systems (MEMS) for biomedical applications, Micromachines 13 (2022). DOI: 10.3390/mi13020164

[3] F. A. Mohd Ghazali, M. N. Hasan, T. Rehman, M. Nafea, M. S. Mohamed Ali, K. Takahata, MEMS actuators for biomedical applications: a review, J. Micromech. Microeng. 30 (2020). DOI: 10.1088/1361-6439/ab8832

[4] G. Bocchetta, G. Fiori, S. A. Sciuto, A. Scorza, Performance of Smart Materials-Based Instrumentation for Force Measurements in Biomedical Applications: A Methodological Review, Actuators 12 (2023). DOI: 10.3390/ACT12070261

[5] S. Bhansali, A. Vasudev (editors), MEMS for Biomedical Applications, Woodhead Publishing, Oxford, 2012, ISBN 9780857096272.

[6] A. K. Basu, A. Basu, S. Ghosh, S. Bhattacharya, (editors), MEMS Applications in Biology and Healthcare, AIP Publishing, 2021, ISBN 9780735423954. DOI: 10.1063/9780735423954

[7] Z. Zhang, X. Wang, J. Liu, C. Dai, Y. Sun, Robotic Micromanipulation: Fundamentals and Applications, Annu. Rev. Control Robot. Auton. Syst. 2 (2019), pp. 181-203. DOI: 10.1146/annurev-control-053018-023755

[8] S. Chowdhury, A. Thakur, P. Švec, C. Wang, W. Losert and S. K. Gupta, Automated Manipulation of Biological Cells Using Gripper Formations Controlled By Optical Tweezers, IEEE Trans. Autom. Sci. Eng. 11 (2014), pp. 338-347. DOI: 10.1109/TASE.2013.2272512

[9] J. Zhang, O. Onaizah, K. Middleton, L. You and E. Diller, Reliable Grasping of Three-Dimensional Untethered Mobile Magnetic Microgripper for Autonomous Pick-and-Place, IEEE Robot. Autom. Lett. 2 (2017), pp. 835-840. DOI: 10.1109/LRA.2017.2657879

[10] N. Chronis and L. P. Lee, Electrothermally activated SU-8 microgripper for single cell manipulation in solution, J. Microelectromech. Syst. 14 (2004), pp. 857-863. DOI: 10.1109/JMEMS.2005.845445

[11] Z. Lyu, Q. Xu, Novel design of a piezoelectrically actuated compliant microgripper with high area-usage efficiency, Precis. Eng. 76 (2022), pp. 1-11. DOI: 10.1016/j.precisioneng.2022.03.003

[12] S. Yang, Q. Xu, A review on actuation and sensing techniques for MEMS-based microgrippers, J. Micro-Bio Robot. 13 (2017), pp. 1-14. DOI: 10.1007/s12213-017-0098-2

[13] Z. Lyu, Q. Xu, Recent design and development of piezoelectric-actuated compliant microgrippers: A review, Sens. Actuators A Phys. 331 (2021), 331: 113002. DOI: 10.1016/j.sna.2021.113002

[14] A. Shelyakov, N. Sitnikov, K. Borodako, V. Koledov, I. Khabibullina, S. von Gratowski, Design of microgrippers based on amorphous-crystalline TiNiCu alloy with two-way shape memory, J. Micro-Bio Robot. 16 (2020), pp. 43-51. DOI: 10.1007/s12213-020-00126-3

[15] F. Beyeler, A. Neild, S. Oberti, D. J. Bell, Y. Sun, J. Dual, B. J. Nelson, Monolithically Fabricated Microgripper With Integrated Force Sensor for Manipulating Microobjects and Biological Cells Aligned in an Ultrasonic Field, J. Microelectromech. Syst. 16 (2007), pp. 7-15. DOI: 10.1109/JMEMS.2006.885853

[16] L. Chen, L. Zhao, H. Wu, L. Pan, Y. Zhao, J. Liu, Design and Analysis of an Electromagnetic Actuated Microgripper for Biomedical Applications, Proc. of the 2023 IEEE Int. Conf. on Real-time Computing and Robotics (RCAR), Datong, China, 3-5 July 2023. DOI: 10.1109/RCAR58764.2023.10249230

[17] H. M. Fard-Vatan, M. Hamedi, Design, analysis and fabrication of a novel hybrid electrothermal microgripper in microassembly cell, Microelectron. Eng. 231 (2020). DOI: 10.1016/j.mee.2020.111374

[18] Y. Zhao, T. Cui, Fabrication of high-aspect-ratio polymer-based electrostatic comb drives using the hot embossing technique, J. Micromech. Microeng. 13 (2003). DOI: 10.1088/0960-1317/13/3/312

[19] Y. Sun, B. J. Nelson, D.P. Potasek, E. Enikov, A bulk microfabricated multi-axis capacitive cellular force sensor using transverse comb drives, J. Micromech. Microeng. 12 (2002). DOI: 10.1088/0960-1317/12/6/314

[20] G. N. Nielson, G. Barbastathis, Dynamic pull-in of parallel-plate and torsional electrostatic MEMS actuators, J. Microelectromech. Syst. 15 (2006), pp. 811-821. DOI: 10.1109/JMEMS.2006.879121

[21] C. Chen, C. Lee, Y. J. Lai, W. Chen, Development and application of lateral comb-drive actuator, Jpn J. Appl. Phys. 42 (2003). DOI: 10.1143/JJAP.42.4059

[22] L. A. Velosa-Moncada, L. A. Aguilera-Cortés, M. A. González-Palacios, J. P. Raskin, A. L. Herrera-May, Design of a novel MEMS microgripper with rotatory electrostatic comb-drive actuators for biomedical applications, Sensors 18 (2018). DOI: 10.3390/s18051664

[23] H. Chang, H. Zhao, F. Ye, G. Yuan, J. Xie, M. Kraft, W. Yuan, A rotary comb-actuated microgripper with a large displacement range, Microsyst. Technol. 20 (2014), pp. 119-126. DOI: 10.1007/s00542-013-1737-8

[24] C. Wang, Y. Wang, W. Fang, X. Song, A. Quan, M. Gidts, H. Zhang, H. Liu, J. Bai, S. Sadeghpour, M. Kraft, Design of a large-range rotary microgripper with freeform geometries using a genetic algorithm, Microsyst. Nanoeng. 8 (2022). DOI: 10.1038/s41378-021-00336-0

[25] R. Crescenzi, M. Balucani, N. P. Belfiore, Operational characterization of CSFH MEMS technology based hinges, J. Micromech. Microeng. 28 (2018). DOI: 10.1088/1361-6439/aaaf31

[26] M. Verotti, R. Crescenzi, M. Balucani, N. P. Belfiore, MEMS-Based Conjugate Surfaces Flexure Hinge, ASME. J. Mech. Des. 137 (2015). DOI: 10.1115/1.4028791

[27] N. P. Belfiore, G. B. Broggiato, M. Verotti, R. Crescenzi, M. Balucani, A. Bagolini, P. Bellutti, M. Boscardin, Development of a MEMS technology CSFH based microgripper, Proc. of the 2014 23rd Int. Conf. on Robotics in Alpe-Adria-Danube Region (RAAD), Smolenice, Slovakia, 3-5 September 2014.
DOI: 10.1109/RAAD.2014.7002273

[28] F. Vurchio, G. Fiori, A. Scorza, S. A. Sciuto, Comparative evaluation of three image analysis methods for angular displacement measurement in a MEMS microgripper prototype: A preliminary study, Acta IMEKO 10 (2021), pp. 119-125.
DOI: 10.21014/acta_imeko.v10i2.1047

[29] T. S. Yallew, N. P. Belfiore, A. Bagolini, M. F. Pantano, Performance Analysis of a CSFH-Based Microgripper: Analytical Modeling and Simulation, Micromachines 25 (2022).
DOI: 10.3390/mi13091391

[30] A. Buzzin, L. Giannini, G. Bocchetta, A. Notargiacomo, E. Giovine, A. Scorza, R. Asquini, G. de Cesare, N. P. Belfiore, On the Dependency of the Electromechanical Response of Rotary MEMS/NEMS on Their Embedded Flexure Hinges' Geometry, Micromachines 14 (2023).
DOI: 10.3390/mi14122229

[31] N. P. Belfiore, A. Bagolini, A. Rossi, G. Bocchetta, F. Vurchio, R. Crescenzi, A. Scorza, P. Bellutti, S. A. Sciuto, Design, Fabrication, Testing and Simulation of a Rotary Double Comb Drives Actuated Microgripper, Micromachines 12 (2021).
DOI: 10.3390/mi12101263

[32] G. Bocchetta, G. Fiori, A. Scorza, N. P. Belfiore, S. A. Sciuto, First results on the functional characterization of two rotary comb-drive actuated MEMS microgripper with different geometry, Proc. of the 25th IMEKO TC4 Symposium and 23rd Int. Workshop on ADC and DAC Modelling and Testing (IWADC), Brescia, Italy, 12-14 September 2022.
DOI: 10.21014/tc4-2022.28

[33] Y. Wei, Q. Xu, An overview of micro-force sensing techniques, Sens. Actuators A Phys. 234 (2015), pp. 359-374.
DOI: 10.1016/j.sna.2015.09.028

[34] G. Bocchetta, G. Fiori, F. Filippi, P. Ursi, S. A. Sciuto, A. Scorza, First results on torque estimation by FEA and experimental analysis in a novel CSFH-based microgripper, Proc. of the 26th IMEKO TC4 Symposium and 24th Int. Workshop on ADC and DAC Modelling and Testing (IWADC), Pordenone, Italy, 20-21 September 2023.
DOI: 10.21014/tc4-2023.42

[35] R. Cecchi, M. Verotti, R. Capata, A. Dochshanov, G. B. Broggiato, R. Crescenzi, M. Balucani, S. Natali, G. Razzano, F. Lucchese, A. Bagolini, P. Bellutti, E. Sciubba, N. P. Belfiore, Development of micro-grippers for tissue and cell manipulation with direct morphological comparison, Micromachines 6 (2015), pp. 1710-1728.
DOI: 10.3390/mi6111451

[36] N. P. Belfiore, M. Verotti, R. Crescenzi, M. Balucani, Design, optimization and construction of MEMS-based micro grippers for cell manipulation, Proc. of the 2013 Int. Conf. on System Science and Engineering (ICSSE), Budapest, Hungary, 4-6 July 2013.
DOI: 10.1109/ICSSE.2013.6614642

[37] F. Botta, M. Verotti, A. Bagolini, P. Bellutti, N. P. Belfiore, Mechanical response of four-bar linkage microgrippers with bidirectional electrostatic actuation, Actuators 7 (2018).
DOI: 10.3390/act7040078

[38] A. Bagolini, S. Ronchin, P. Bellutti, M. Chistè, M. Verotti, N. P. Belfiore, Fabrication of Novel MEMS Microgrippers by Deep Reactive Ion Etching With Metal Hard Mask, J. Microelectromech. Syst. 26 (2017), pp. 926-934.
DOI: 10.1109/JMEMS.2017.2696033

[39] T. Chen, L. Sun, L. Chen, W. Rong, X. Li, A hybrid-type electrostatically driven microgripper with an integrated vacuum tool. Sens. Actuators A Phys. 158 (2010), pp. 320-327.
DOI: 10.1016/j.sna.2010.01.001

[40] Y. S. Oh, W. H. Lee, H. E. Stephanou, G. D. Skidmore, Design, optimization, and experiments of compliant microgripper, in Proc. of the ASME 2003 Int. Mechanical Engineering Congress and Exposition. Microelectromechanical Systems. Washington, DC, USA, 15-21 November 2003.
DOI: 10.1115/IMECE2003-55013

[41] T.E. Rudenko, A.N. Nazarov, V.S. Lysenko, The advancement of silicon-on-insulator (SOI) devices and their basic properties, Semicond. Phys. Quantum Electron. Optoelectron. 23 (2020), pp. 227-252.
DOI: 10.15407/spqeo23.03.227

[42] G. Bocchetta, G. Fiori, A. Scorza, S. A. Sciuto, Image quality comparison of two different experimental setups for MEMS actuators functional evaluation: a preliminary study, Proc. of the 25th IMEKO TC4 Symposium and 23rd Int. Workshop on ADC and DAC Modelling and Testing (IWADC), Brescia, Italy, 12-14 September 2022.
DOI: 10.21014/tc4-2022.59

[43] F. Vurchio, G. Bocchetta, G. Fiori, A. Scorza, N. P. Belfiore and S. A. Sciuto, A preliminary study on the dynamic characterization of a MEMS microgripper for biomedical applications, Proc. of the 2021 IEEE Int. Symposium on Medical Measurements and Applications (MeMeA), Lausanne, Switzerland, 23-25 June 2021.
DOI: 10.1109/MeMeA52024.2021.9478703

[44] A. Masolin, P. O. Bouchard, R. Martini, M. Bernacki, Thermo-mechanical and fracture properties in single-crystal silicon, J. Mater. Sci. 48 (2013), pp. 979-988.
DOI: 10.1007/s10853-012-6713-7

[45] M. A. Hopcroft, W. D. Nix, T. W. Kenny, What is the Young's modulus of silicon?, J. Microelectromech. Syst. 19 (2010), pp. 229-238.
DOI: 10.1109/JMEMS.2009.2039697

[46] B. Bhushan, X. Li, Micromechanical and tribological characterization of doped single-crystal silicon and polysilicon films for microelectromechanical systems devices, J. Mater. Res. 12 (1997), pp. 54-63.
DOI: 10.1557/JMR.1997.0010

[47] P. Ursi, A. Rossi, F. Botta, N. P. Belfiore, Analytical Modeling of a New Compliant Microsystem for Atherectomy Operations, Micromachines 13 (2022), pp. 1094-1123.
DOI: 10.3390/mi13071094

[48] J. Liu, N. A. Abu Osman, M. Al Kouzbary, H. Al Kouzbary, N. A. Abd Razak, H. N. Shasmin, N. Arifin, Stiffness estimation of planar spiral spring based on Gaussian process regression", Sci. Rep. 12 (2022), pp. 1-15.
DOI: 10.1038/s41598-022-15421-1

[49] A. Cammarata, P. D. Maddio, R. Sinatra, N. P. Belfiore, Direct Kinetostatic Analysis of a Gripper with Curved Flexures, Micromachines 13 (2022).
DOI: 10.3390/mi13122172

[50] M, Verotti, A. Dochshanov, N. P. Belfiore, Compliance synthesis of CSFH MEMS-based microgrippers, J. Mech. Des. 139 (2017).
DOI: 10.1115/1.4035053

[51] A. Buzzin, A. Veroli, G. De Cesare, N. P. Belfiore, Nems-technology based nanogripper for mechanic manipulation in space exploration missions, Proc. of the 4th IAA Conf. on University Satellite Missions and CubeSat Workshop, Rome, Italy, 4-7 December 2017, Advances in the Astronautical Sciences Volume 163, 2018, pp. 61-67.

[52] N. P. Belfiore, P. Simeone, Inverse kinetostatic analysis of compliant four-bar linkages. Mech. Mach. Theory 2013, 69, pp. 350–372.

[53] J. R. Taylor, An introduction to Error Analysis: The study of Uncertainties in Physical Measurements, University Science Books, New York, 1997, ISBN: 9780935702422.

[54] P. N. Prasad, Introduction to Biophotonics, John Wiley & Sons, Hoboken, 2003. ISBN: 9780471287704.

[55] G. Fiori, G. Bocchetta, S. Conforto, S. A. Sciuto, A. Scorza, Sample volume length and registration accuracy assessment in quality controls of PW Doppler diagnostic systems: a comparative study, Acta IMEKO 12 (2023)2, pp. 1-7.
DOI: 10.21014/actaimeko.v12i2.1425

[56] G. Fiori, F. Fuiano, A. Scorza, J. Galo, S. Conforto, S. A. Sciuto, A preliminary study on an image analysis based method for lowest detectable signal measurements in Pulsed Wave Doppler ultrasounds, Acta IMEKO 10 (2021) 2, pp. 126 - 132. DOI: 10.21014/acta_imeko.v10i2.1051

[57] C. E. Papadopoulos, H. Yeung, Uncertainty estimation and Monte Carlo simulation method, Flow Meas. Instrum. 12 (2001), pp. 291-298. DOI: 10.1016/S0955-5986(01)00015-2

[58] M. Huff, Recent advances in reactive ion etching and applications of high-aspect-ratio microfabrication, Micromachines 12 (2021). DOI: 10.3390/mi12080991

[59] T. Xu, Z. Tao, H. Li, X. Tan, H. Li, Effects of deep reactive ion etching parameters on etching rate and surface morphology in extremely deep silicon etch process with high aspect ratio, Adv. Mech. Eng. 9 (2017). DOI: 10.1177/1687814017738152

[60] B. Nöhammer, C. David, H. Rothuizen, J. Hoszowska, A. Simionovici, Deep reactive ion etching of silicon and diamond for the fabrication of planar refractive hard X-ray lenses, Microelectron. Eng. 67-68 (2003), pp. 453-460. DOI: 10.1016/S0167-9317(03)00101-1

[61] S. D. Senturia, Microsystem design, Springer, New York, 2005, ISBN 9780306476013.

[62] H. Chang, H. Zhao, F. Ye, G. Yuan, J. Xie, M. Kraft, W. Yuan, A rotary comb-actuated microgripper with a large displacement range, Microsyst. Technol. 20 (2014), pp. 119-126. DOI: 10.1007/s00542-013-1737-8

[63] O. Baer, C. Giusca, R. Kumme, A. Prato, J. Sander, D. Mirian, F. Hauschild, Digital Twin concept of a force measuring device based on the finite element method, Acta IMEKO 12 (2023)1, pp. 1-5. DOI: 10.21014/actaimeko.v12i1.1404

[64] M. Verotti, P. Di Giamberardino, N.P. Belfiore, O. Giannini, A genetic algorithm-based method for the mechanical characterization of biosamples using a MEMS microgripper: numerical simulations, J. Mech. Behav. Biomed. Mater. 96 (2019), pp. 88-95. DOI: 10.1016/j.jmbbm.2019.04.023